CHAPTER 2: OVERVIEW OF MODELS AND METHODOLOGY

The San Francisco Bay region (SFBR) sits within the Pacific-North American plate boundary (**Figures 2.1, 2.4**). About 80 percent of the total plate boundary slip occurs across a 150 km-wide zone extending from the Farallon Islands to the west edge of the Central Valley, with most of this deformation occurring in an even narrower (50 km-wide) zone spanning the San Andreas and Calaveras Fault zones. The SFBR has the highest density of active faults and the highest rate of seismic moment release per km^2 of any urban area in the United States. The SFBR has experienced many sizeable and damaging earthquakes, including six magnitude **M**≥6.5 events in 1836, 1838, 1865, 1868, 1906, and 1989 (**Figure 2.2**) with magnitudes of 6.5, 6.8, 6.5, 6.8, 7.8, and 6.9, respectively.

The earthquake history of the SFBR has been documented in detail by Bakun (1999) and is believed to be complete for **M**≥5.5 events since 1850 (**Figure 2.2**), when the population of the SFBR increased greatly due to the discovery of gold in the Sierra foothills east of Sacramento. In the context of this study, three important observations can be made of this earthquake history. First, four **M**≥6.7 earthquakes have occurred in the historical record. Four events since 1838 corresponds to a rate of occurrence for **M**≥6.7 events in the SFBR of between 0.020/yr and 0.024/yr. Second, Bakun (1999) has shown that the size distribution of earthquakes in the SFBR corresponds to b=0.9 in the Gutenberg-Richter representation, both for the larger events since 1850 and for smaller events in the 20th Century.

Finally, the rate of earthquakes in the SFBR was considerably higher before 1906 than after (**Figure 2.2).** For the 70 years before 1906, 17 **M**≥6 earthquakes occurred in the SFBR while in the 95 years after 1906 there have been only five (Ellsworth and others, 1981; Bakun, 1999). We estimate the chance of this change in rate being due to random fluctuations to be less than 5%. The post-1906 seismic quiescence is thought to be due to a "stress shadow" cast by the 1906 earthquake over much if not all of the SFBR (Harris and Simpson, 1998). Both large and small earthquakes can be suppressed by the occurrence of a nearby earthquake, and can remain suppressed until the faults in the region are sufficiently reloaded (e.g., Harris and Simpson, 1998). In the SFBR, reloading occurs as the Pacific Plate moves northwestward past the North American Plate. In the SFBR, most of the major faults were relaxed to some degree by the 1906 earthquake, owing to the great length of its rupture and the sub-parallel, strike-slip geometry of these faults (R.W. Simpson, Appendix F).

There is no consensus within WG02, however, as to whether the SFBR remains within the 1906 stress shadow, as suggested by seismicity data for the past 96 years; is now emerging from it, as suggested by calculations based on rheological models of the crust and uppermost mantle; or has emerged from 1906 effects, as suggested by the simplest elastic interaction models. This area of uncertainty has led to substantial differences between the analysis reported by WG99 and that reported here. Put another way, the stress shadow cast over the SFBR by the 1906 San Francisco earthquake has, in turn, cast a considerable cloud of uncertainty over the deliberations and findings of Working Group 2002.

Uncertainty is no stranger to assessments and projections in the Earth Sciences, but it has rarely been an honored guest at these functions. WG02 has devoted considerable effort to defining uncertainties in the data, models, and parameters exercised here; quantifying these uncertainties; and tracking them throughout the calculations. In any model, there may be two types of uncertainty: *aleatory uncertainty* and *epistemic uncertainty*. Aleatory uncertainty refers to the random variability that occurs in the natural world. The throwing of dice is the classic example, perhaps because the word aleatory has its etymological origins in the Latin word for dice. Epistemic uncertainty refers to what we don't know about the natural world, our ignorance of how the Earth works to manufacture earthquakes of a certain size at a certain place and time, for example. The differing opinions on the present-day effects of the 1906 stress shadow are a measure of epistemic uncertainty about this matter. To the extent a process is knowable, its epistemic uncertainty is reducible. Aleatory uncertainty, on the other hand, while quantifiable through direct observation of the phenomena of interest, is irreducible. WG02 uses *models* (sometimes more than one) to calculate quantities, and these models are defined by *parameters* that must be estimated. Both the choice of models and estimation of their parameters have uncertainty associated with them. These *model uncertainties* and *parameter uncertainties* are, in general, of both the aleatory and epistemic types. Finally, WG02 uses *expert opinion* to decide a number of matters in this report. Differing expert opinion also represents uncertainty. Insofar as such differences arise from differing evaluations or perceptions of available but incomplete knowledge (for example, the varying interpretations of the present-day effects of the 1906 stress shadow), this uncertainty is of the epistemic type.

Almost all of the uncertainty considered in this report, including that arising from diverse expert opinion, is treated as epistemic uncertainty. (The only exceptions are the event-to-event variability that we associate with magnitude distributions, natural variability in which fault segments combine to create earthquakes, and the aleatory component of the uncertainty in our time-dependent probability models.) Confronted with a range of possibilities for a parameter (for example, the length of a fault segment) or a relation (for example, the relation between segment area and earthquake magnitude) or a probability model, WG02 uses multiple choices with weights assigned to reflect the uncertainty. To sample systematically among the vast number of combinations of the weighted choices for input data and models, WG02 employs a Monte Carlo technique (also described as a logic-tree approach) in which thousands of complete calculations for SFBR earthquakes and their probability are made. From the distribution of the calculation results, we obtain various mean values (for example, long-term rupture rates or 30-year earthquake probabilities) and their 90% and 95% confidence bands.

An example of how weighted choices are used to represent uncertainty is shown in **Figure 2.3** for the case of estimating the seismogenic area and seismic moment rate (and their uncertainties) for the North Hayward Fault segment, given sets of weighted choices for segment length L, segment width W, seismic slip factor R and slip rate v. (This calculation is described more fully in **Chapter 4**.) The result calculated using the preferred values is near or at the maximum of the distribution function for all possible results, as we would expect. Uncertainties in the calculated results can be large, however, if high confidence levels are imposed on the results. Every result presented in **Chapter 6** is stated as a mean value and its 95% confidence band, as inferred from the Monte Carlo sampling.

The earthquake probabilities reported here are the results of a set of model calculations consisting of three basic elements. The first element is the *SFBR earthquake model* (described more fully in **Chapter 4**) which determines the average, long-term rate of earthquakes on the principal faults. The second element is the set of "background" earthquakes, those earthquakes that occur in the SFBR on faults either uncharacterized or unrecognized by this study, the probability for which is based on historical seismicity rates extrapolated to **M**≥6.7 events. The third element of these calculations is a suite of *probability models*, which are described in **Chapter 5**. The probability models range from the simplest (a time-independent Poisson model) to those that incorporate certain time-dependent physical aspects of the causes and effects of earthquakes, such as the progression of faults through an "earthquake cycle" and the interactions of faults through their stress fields.

Because of the inclusive approach taken by WG02 toward all forms of uncertainty and differing expert opinion, the model used by WG02 to calculate earthquake probability is complex. This complexity notwithstanding, certain assumptions and parts of the model play critical roles in the calculation and strongly affect the results, while others affect the results only a little. In the remainder of this chapter, we introduce the key elements of the WG02 model, paying particular attention to those things that matter most in calculating the earthquake probabilities in the SFBR.

SFBR Earthquake Model

For the purposes of this study, the San Francisco Bay Region (SFBR) is a rectangular region, extending from Santa Rosa on the north to Monterey on the south, which trends parallel to the northwesterly strike of the principal faults of the San Andreas system and which includes them all (**Figure 2.4**). From west to east, they are the San Gregorio, San Andreas, Hayward-Rodgers Creek, Calaveras, Concord-Green Valley, and Greenville Faults, plus the Mt Diablo Thrust, a blind thrust lying between the northern end of the Calaveras Fault and the southern end of the Concord-Green Valley Fault. These seven faults are referred to as the *characterized faults* in this study.

Attached to the SFBR is a panhandle extending along the San Andreas Fault to Cape Mendocino. This extension is needed to mechanically accommodate in our model long ruptures of the San Andreas Fault, such as that which occurred in 1906. However, when we report results for the SFBR herein, they reflect only earthquakes occurring in or extending into the rectangular SFBR region.

The SFBR earthquake model is fundamentally a geologic model in that both its geometry and long-term behavior are defined and constrained by geologic observation. The model incorporates complexity that leads to a wide spectrum of earthquake sizes, and includes both fault-by-fault and regional constraints on the frequency of occurrence of these earthquakes based on geologic and geodetic observations of slip rate. The basic elements of the SFBR earthquake model are introduced in the box below, and more fully discussed in **Chapters 3 and 4**.

The SFBR Earthquake Model

Fault segments
The SFBR model is built upon the seven characterized faults mentioned above . Each fault is divided into as many as four, non-overlapping segments – 18 segments in all. These segments are the basic building blocks for earthquake ruptures on each fault. Each *fault segment* has length *L*, width *W*, geologic slip velocity *v*, and seismogenic scaling factor *R*, which accounts for any part of the geologic slip that is aseismic (**Figure 2.5**, **Table 3.8**).

Rupture sources
Unlike WG90, which considered only single-segment ruptures, the present study allows for the simultaneous rupture of two or more adjacent segments of a fault. Each possible combination of segments is a *rupture source*. These rupture sources—35 in all—are listed in **Table 4.8**. A mean magnitude is computed for each *rupture source* based on its seismogenic area *A* (determined by *L*, *W*' and *R* on each of its segments) through "**M**–log *A*" relations, as described in **Chapter 4**.

Floating earthquakes
Each fault (except Mt. Diablo) is host to *floating earthquakes*—earthquakes of a specified magnitude but without a fixed location. Floating earthquakes, which allow for the fact that some earthquakes are not represented by the prescribed segmentation, are also classified and treated as *rupture sources* and are listed in **Table 4.3**.

Rupture scenarios
A *rupture scenario* is a combination of rupture sources that describes a possible mode of failure of the entire fault during one earthquake cycle. For example, in one rupture scenario the Hayward-Rodgers Creek Fault fails only in 3-segment ruptures, in another it fails only in single-segment ruptures, and in a third scenario it fails in combinations of 1-segment and 2-segment ruptures (**Table 3.4**).

Fault rupture models
A fault rupture model us a weighted combinations of the rupture scenarios for a fault, each combination representing one possibility for the long-term behavior of the fault. The weights are determined by expert opinion. The *fault rupture model*s serve the same function as the "earthquake-cascade" models employed in WG95 (SCEC, 1995). For most faults, multiple fault rupture models are considered.

Regional model
A viable *regional model* is an aggregate of seven *rupture models* (one for each fault) and a *background earthquake model* (described below) that satisfies a plate-motion slip rate constraint across the entire SFBR defined by geodetic observations. A *regional model* provides a complete description of the long-term earthquake activity in the SFBR.

Background Earthquakes

Earthquakes that have occurred (and will occur) within the SFBR on structures other than the seven characterized faults are termed *background earthquakes*. Numerous known faults and structures in the SFBR not characterized here are considered capable of producing **M**≥6.7 earthquakes, as are, presumably, some yet-unrecognized faults and structures at depth in the SFBR (for example, prior to 1989, the source of the Loma Prieta earthquake).

Like the *characterized earthquakes*, background earthquakes have their origins in the elastic strain accumulation driven by the relative motions of the North American and Pacific plates. As described more fully in **Chapter 4**, the SFBR accommodates about 40 mm/yr of strike-slip plate motion (De Mets and Dixon, 1999; Prescott et al., 2001) and about 4 mm/yr of convergent plate motion (Prescott et al., 2001. Almost all of the strike-slip plate motion occurs on the *characterized faults* (excluding the Mt. Diablo thrust) but some also occurs in background earthquakes. The accommodation of plate tectonic motion by earthquakes of various types is schematically illustrated in **Figure 2.6**.

WG02 characterizes only one geologic structure that can accommodate appreciable convergent plate motion—the Mt. Diablo Thrust. Given the small dimension of this structure compared to the 220-km along-strike length of the SFBR, the Mt. Diablo Thrust can account for only a small fraction of the convergent plate motion. Convergent background earthquakes also accommodate convergent plate motion. These may occur in other regions of local uplift associated with thrust faults, along the eastern edge of the Great Valley, for example, or the west side of the Santa Clara Valley (**Figure 2.7**).

Background earthquakes of both the strike-slip and convergent types are considered here in terms of a Gutenberg-Richter distribution with b=0.9, $\mathbf{M}_{max}$ =7.25 ±0.25, and a constant rate of occurrence defined by the rates in the historical and instrumental records. WG02 does not apply a strain accumulation/release (moment-balance) constraint to the background earthquakes, as we do for earthquakes on characterized faults.

Probability Models

An earthquake probability model describes the time-dependence of earthquake occurrence. After the mean rupture rates and magnitudes are calculated for rupture sources in the SFBR, they become input for the several probability models used in this study and described more fully in **Chapter 5**. Different probability models incorporate different physical attributes of the earthquake process.

In calculating earthquake probabilities in the SFBR, WG02 recognizes two essential, time-dependent aspects of the causes and effects of earthquakes, the first relating to the earthquake cycle and the second to fault interactions. The concept of the earthquake cycle has its origins in the elastic-rebound hypothesis, first formulated for the 1906 earthquake and its likely successor on the San Andreas Fault (Reid, 1908). It holds that after a major earthquake and its immediate aftershocks, another major earthquake on the same reach of fault is not possible until elastic strain has re-accumulated in an amount comparable to that released in the previous major

earthquake. As time goes on and more and more elastic strain accumulates, the next large earthquake becomes increasingly likely. If the SFBR had only the San Andreas Fault and 1906-type earthquakes to account for, quantifying these effects would be far simpler (although not necessarily accurate with available data). But this is not the case. Smaller-magnitude but still large earthquakes, perhaps with their own "earthquake cycles," have occurred on or near the reach of the San Andreas Fault that ruptured during the 1906 earthquake, both before (in 1838) and after (in 1989) this event.

With respect to fault interactions, it is necessary to estimate the effects of the 1906 earthquake on the other SFBR faults, as well as similar (but smaller and more localized) effects of the Loma Prieta earthquake (Oct. 17, 1989; **M** = 6.9). Both model calculations and known seismicity rates since 1836 (**Figure 2.2**) suggest that the 1906 earthquake cast a deep and long-lasting "stress shadow" across the entire SFBR (see, for example, Harris and Simpson, 1998). As noted previously, however, there is no consensus as to whether the SFBR remains within the 1906 stress shadow, is now emerging from it, or is well removed from 1906-related effects.

All of this lends considerable uncertainty to the probability estimates reported here–uncertainty in addition to that contained in the SFBR earthquake model. This uncertainty is expressed both in the range of probability models described below and in the expert opinion applied to them in the form of relative weights.

The first of the five probability models used to determine earthquake probabilities in the SFBR is the *Poisson* model. Poisson probabilities do not vary with time and are fully determined by the mean rates of earthquakes in the SFBR regional model.

The *Empirical* model is a variation of the *Poisson* model. It incorporates time-dependence by modulating the average rates of rupture sources with the current regional rate of seismicity, which is currently lower than its long-term average. The *Empirical* model thus uses modern seismicity rates as a proxy for stress shadow calculations that rely on poorly known rheological/mechanical properties of the crust and uppermost mantle under the SFBR. Inclusion of the *Empirical* model is a significant departure from the approaches toward probability modeling taken by WG90 and WG99.

The *Brownian Passage Time* (BPT*)* and *Time-Predictable* (TP) models used in this study are both time-dependent probability models. In BPT model, the failure condition of a fault or fault segment is specified by a state variable, which rises from a ground state to the failure state in the course of the earthquake cycle. Evolution of this model toward failure is governed by a deterministic parameter reflecting the reloading rate of the fault or fault segment and a stochastic parameter α, or "aperiodicity", that allows for random variations in the process. The "stress shadow" effects of nearby earthquakes are admitted in the BPT model through steps in the state variable calculated with elastic interaction models. The TP model requires that both the date and the amount of slip of the most recent earthquake be known. In this model, the expected time of the next characterized earthquake is equal to the time required for the strain accumulation process to provide for the same amount of faulting displacement as occurred in the previous event. The TP model is applied here only to segments of the San Andreas Fault that ruptured in

the 1906 earthquake; this is the only SFBR earthquake for which detailed slip measurements are available.

How the inherent randomness of the earthquake process is modeled affects the probability calculations for all of the rupture sources. We estimated α from 37 sequences of repeating earthquakes to be in the range 0.3–0.7, similar to the the cov of 0.5±0.2 used by WG95. This is in contrast to smaller values used by WG88 and WG90 based on the work of Buland and Nishenko (1987), and it is fair to say that the estimation of α remains a significant scientific challenge and a significant source of uncertainty in time-dependent earthquake forecasting. The effect of α on WG02's probability calculations depends on the time since the most recent rupture. For the 30-year period 2002-2031, assuming greater randomness decreases the probability on most of the faults, but increases the probability of earthquakes on the San Andreas Fault.

Expert Opinion

Expert opinion has been used in seismic hazard and risk analyses for more than two decades. For most earth scientists, the theory and practice of expert opinion will come as new developments, but WG02 believes that the basic principles are consonant with the philosophy of multiple working hypotheses (multiple working models, in the case of this report). Earth scientists have long embraced the use of multiple working hypotheses when knowledge is insufficient to eliminate any of them (Gilbert, 1886; Chamberlin, 1890). In this approach, experts are convened to define and portray the body and range of informed opinion on the matter at hand (SSHAC, 1997; Hanks, 1997). The process should be inclusive: that is, any other group of experts should express the same range of knowledge and models. The " truth" or "right answer" is assumed to lie somewhere among or between the various opinions. In this context it is not useful to try to decide which experts are "right" and which experts are "wrong" because there is no way of knowing. If there were, there would be no need for all the experts in the first place. Finally, all should recognize that experts are not convened to reduce uncertainty; indeed, in their differing opinions, they are the source of much of it.

This report is not a *consensus report,* at least not in the sense that previous reports on California earthquake probabilities (1988, 1990, 1995) were consensus reports. In particular, WG02 does not arrive at final probability numbers by agreeing in advance on a single model or method for calculating them. Rather, this report proceeds on the basis of a *consensus process,* which admits a variety of models that are significantly different from one another, for one reason or another. The final result is determined by the aggregated expert opinion expressed individually by the 13 members of the *Overview Group* of WG02, which had responsibility for contents and conclusions of this report. The members of that group are listed at the beginning of this report.

The SFBR earthquake model is a *consensus feature* of this study. WG02 uses only this model to estimate earthquake rates as a function of size on a fault-by-fault and segment-by-segment basis, even though other models, such as the cascade model of WG95 or the models of Ward (2000) and Andrews and Schwerer (2001), do similar things. Surely, therefore, there is some uncertainty associated with the adoption of this single model that is left unquantified here. Perhaps the segmentation basis of the analysis here is incorrect, or perhaps the choices of segments are

incorrect, or perhaps the proscription against ruptures of only a part of a segment (apart from floating earthquakes) is incorrect. If so, WG02 has no way of knowing by how much. What we can do is compare the SFBR model predictions of average earthquake occurrence rates to what is known to us through the historical and prehistoric records of earthquakes. The SFBR earthquake model passes these tests, but so do other models.

The Strain Accumulation/Release Constraint

Earthquakes in the San Francisco Bay Region have their origins in the elastic strain energy accumulating in the region due to the steady motion of the Pacific plate relative to the North American plate. Most of this relative motion is in the form of horizontal shear of 36-43 mm/yr across the SFBR and is released on faults in strike-slip earthquakes.

Both the accumulation and release of strain energy are measurable quantities for the San Francisco Bay Region (Bakun, 1999; Prescott and others, 2001). There are long-term and short-term estimates for each (**Figure 2.8**). In terms of slip velocity across the region, the long-term accumulation inferred from global plate motion models is 41±1 mm/yr (De Mets and Dixon, 1999). This value is an average over the past five million years, and has been corrected for the San Francisco Bay by subtracting contributions of Great Basin extension and motion of the Sierra Nevada-Great Valley block from the full relative motion of the Pacific and North American plates. The short-term accumulation rate measured using GPS data for the past seven years is in good agreement at 39.8±1.2 mm/yr (Prescott and others, 2001).

Long-term release of strain energy on individual faults is measured by the faults' geologic slip rates averaged over thousands—often many thousands—of years. Sums of the slip velocity measured on strike-slip faults in the SFBR can be compared to the plate-motion rate (**Figure 2.9**). Finally, the short-term release of strain energy can be estimated from the historical record of earthquakes in the SFBR. The seismic moment sum for the period 1850 to present corresponds to a mean slip velocity of roughly 31 mm/yr. A large uncertainty—approximately 50% of this value—arises primarily from uncertainty in the seismic moment of the 1906 earthquake, which alone has contributed about two thirds of SFBR seismic moment sum since 1850 (Bakun, 1999).

The coincidence of these four very different measures of slip velocity reveals that what goes into the SFBR in the way of plate motion strain energy accumulation comes out as strain energy release, whether this is measured by geologic fault slip rates or by the seismic moment sum of the historical record of earthquakes. These estimates of strain energy accumulation and release are in remarkably good agreement on both the long term and, even more surprisingly, on the short term.

From Segments to Earthquakes

WG02's method for estimating the size of earthquakes on the characterized faults (including both single-segment and multiple-segment ruptues) uses the fault area A to estimate moment magnitude **M**. Seismic moment M_0 for each event is then determined from the inverse of the moment magnitude relation (Hanks and Kanamori, 1979)

$$\log M_0 = 3/2\ \mathbf{M} + 16.05. \qquad (2.1)$$

To put the strain accumulation/release constraint of the last section into play, the seismic moment sum for each characterized fault is computed. These sums are balanced against the total moment rate defined by areas and geologic slip velocities determined for segments involved.

We use three sets of **M**–log A relations in this analysis: that of Wells and Coppersmith (1994); those developed originally by W.L. Ellsworth for WG99 and reproduced here in Appendix D; and those of Hanks and Bakun (2002) invoking L-model scaling of fault slip at **M**≥7. The differences between these relations make for the principal source of uncertainty in the SFBR earthquake model. Even modest differences (or uncertainties) among these relations (say 0.2 units in **M**) provide for a factor of 2 difference (or uncertainty) in M_0 and therefore in the rates of such earthquakes, given the moment-balanced format of our calculations.

In addition to the **M**–log A relations, several other considerations play key roles in determining the long-term average rate of earthquakes and their size distribution. Aseismic slip, or fault creep, comes into play through the *seismogenic factor R*, the ratio of seismogenic fault slip to total fault slip, by reducing the effective area of the rupture sources in the model (**Appendix B**). Generally, where the *R* factor reduces the rupture area, it reduces the earthquake magnitude. For some of the shorter fault segments having significant amounts of aseismic slip, such as those on the Hayward, Calaveras, and Concord-Green Valley Faults, magnitudes associated with single-segment ruptures can be and often are **M**<6.7. Thus, it is important to distinguish between the rates of **M**≥6.7 earthquakes, which is our principal concern in this analysis, and *segment-rupture rates*, which include all of the rupture sources involving a given segment, including those with **M**<6.7. Segment-rupture rates may be more useful than **M**≥6.7 earthquake rates for interpreting geologic, site-rupture data for paleo-earthquakes with **M**~6.7.

A third factor controlling the rates of earthquakes in the SFBR model are the various *rupture scenarios* and *rupture models*. These are important features in moment-balanced calculations such as these, because the seismic moments of just a few large earthquakes will typically dominate the total moment for a segment, for a fault, or for the SFBR as a whole. Finally, the choice of **M** for the *floating earthquakes* may or may not be an important contributor to the total moment for that segment, depending on the floating earthquake's size relative to the size of the segment-rupturing earthquakes on that fault.

The Calculation Sequence

The Calculation Sequence (CS), described more fully in **Chapter 4**, is the computational apparatus that embodies the SFBR earthquake model, the background earthquake model, and the probability models, and calculates the earthquake probabilities. The CS first calculates average rates of rupture sources on the characterized faults. These rates, in turn, are the input to each of the five probability models. The rates of background earthquakes are calculated with a Gutenberg-Richter model for the SFBR as a whole; probabilities for the background earthquakes are calculated only for the Poisson probability model.

The CS is illustrated schematically in **Figures 2.10 and 2.11**. Calculation of the rates of rupture sources is shown in **Figure 2.10**, beginning with the segment geometry and creep rates on the left and concluding with rupture rates on the right. Along the way, we calculate **M** and M_0 for each rupture source in the bottom path of **Figure 2.10**. In the top path we calculate seismic moment rates for each segment and each rupture model through their ΣM_0's, constraining them both locally and regionally according to individual fault slip rates and the plate-motion rate, respectively. The resulting rupture source rates are then input to the probability models (**Figure 2.11**).

Implicit in these schematic diagrams are the multiple choices of numerous parameters and models involved in these calculations and their assigned weights. For example, as illustrated in **Figure 2.3**, the seismogenic area A of a fault segment is calculated from the product of its length *L*, width *W*, and seismogenic scaling factor *R*. Its length, in turn, is calculated from the geographic coordinates of the segment's endpoints. The uncertainty in each of these parameters (each *L* endpoint location, *W*, and *R*) is represented by three branches. Thus, there are 81 (3^4) paths through this part of the CS, yielding 81 measures of the seismogenic area. The most likely measure is that found for the highest-weighted branch choices, but the less likely paths are also followed in the Monte Carlo sampling of the CS. Put another way, each choice of these parameters, together with the weight assigned to it by WG02, occupies a branch of the logic tree. WG02 often assumes that the uncertainty in a parameter is normally distributed, and represents the mean and width of the distribution with three branches (or occasionally five) and their respective weights (corresponding to either the 90% and 95% uncertainty bounds), as given in **Table 2.2**.

Table 2.2: Branch weights corresponding to mean and 90% and 95% bounds for parameter estimates.

Uncertainty bound	Branch weights				
90% (±1.64 sigma)	0.185		0.63		0.185
	0.13		0.74		0.13
95% (±1.96 sigma)					
	0.09	0.16	0.50	0.16	0.09

Similarly, *alternate models* for a calculation—for example, the several **M**–log *A* models—are also represented by multiple branches in the logic tree, but with weights assigned by expert opinion. The number of possible paths through the whole CS is huge. WG02 explores the range of possible behaviors with a random sampling or Monte Carlo technique. The results of the CS—the calculated probabilities of earthquakes—are described in **Chapter 6**. For each result we report the mean and 95% confidence range for a suite of 10,000 model realizations. Through repeated testing of the code we have determined this number to be more than sufficient to ensure that mean and uncertainty bounds are well determined. The CS is carried out in a Fortran 77 program that is described in **Appendix G**.

Figure 2.1. Major faults of the San Francisco Bay Region. Arrows show the mostly strike-slip sense of tectonic plate motion accommodated by earthquakes and aseismic creep on SFBR faults. Yellow lines indicate extent of rupture in the 1868 **M**~6.8 earthquake on the southern Hayward faults and that in the 1989 **M**6.9 Loma Prieta earthquake near the San Andreas fault northeast of Monterey Bay.

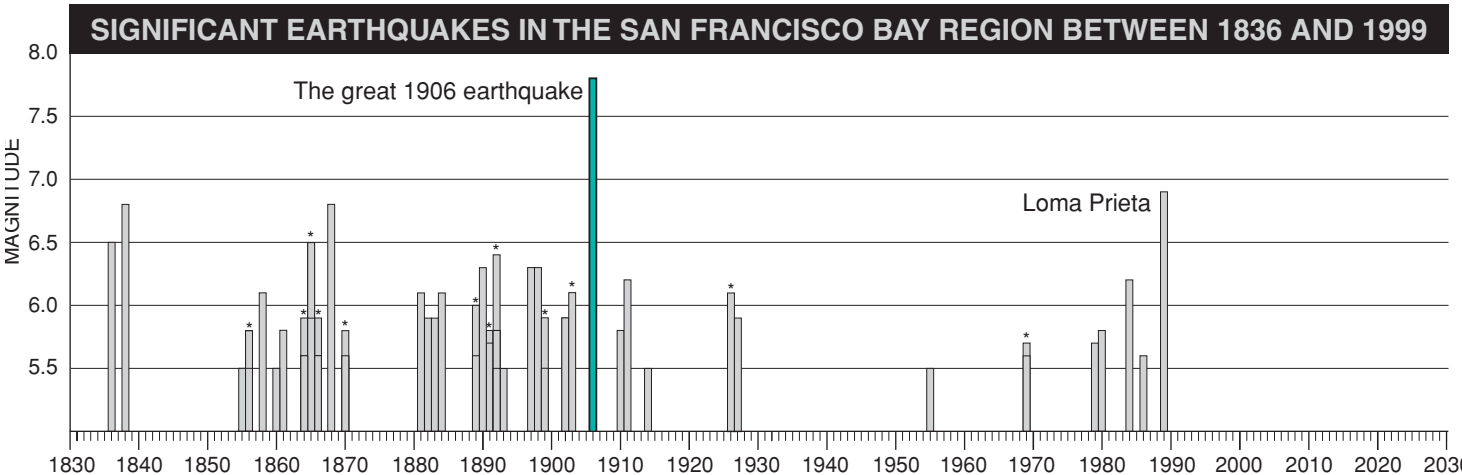

Figure 2.2. Time sequence of earthquakes M >= 5.5 in the SFBR since the early 19th century, from the catalog of Bakun (1999) The catalog is believed to be complete for such magnitude earthquakes since 1850. A high rate of earthquake activity in the late 1800's was followed by relatively little activity after 1906. Asterisk indicates more than one earthquake occurred that year.

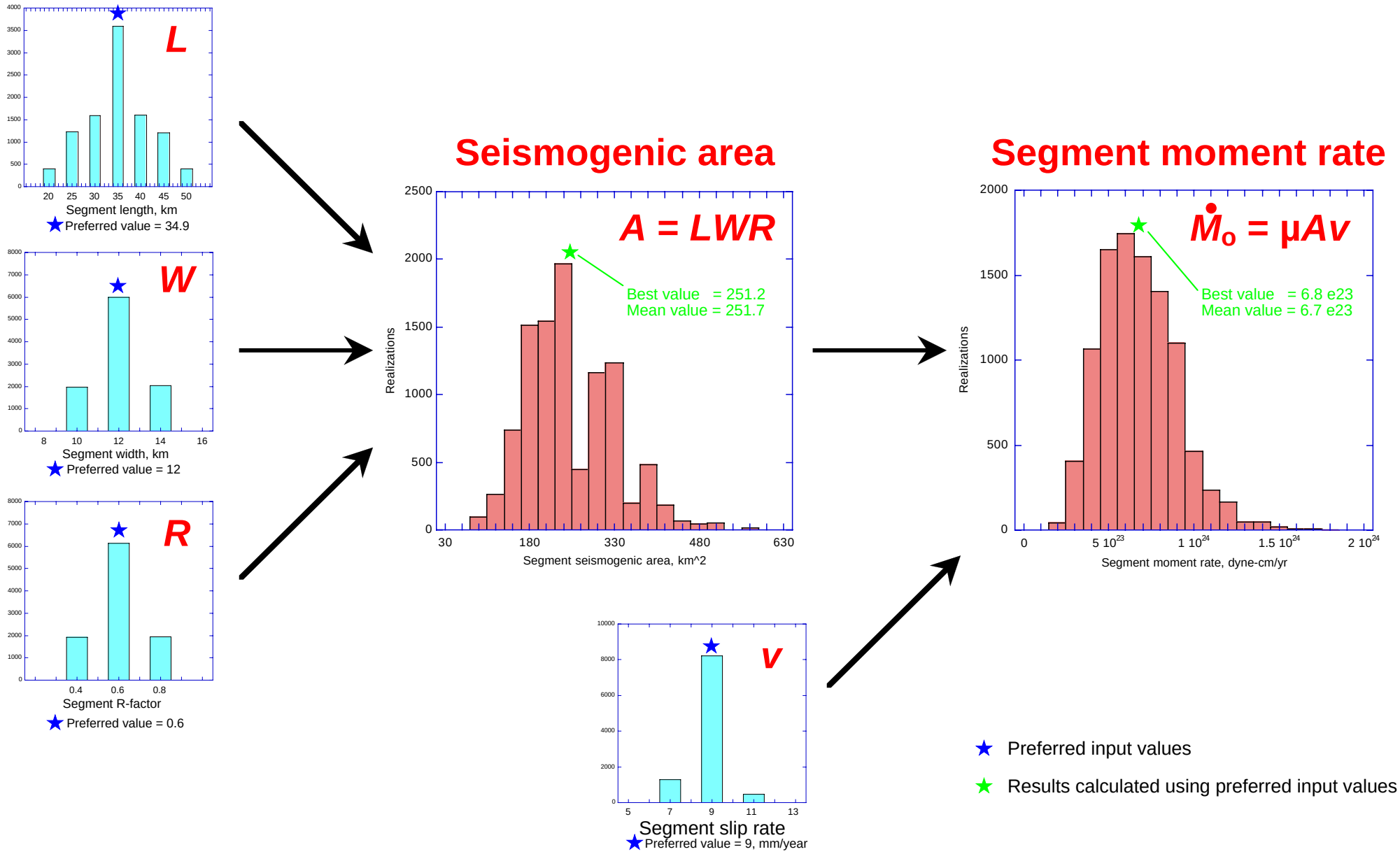

Figure 2.3. Illustration of WG02's approach to model calculations. Blue histograms show values and frequencies of fault segment length L, width W, seismogenic scaling factor R, and slip rate v. Red histograms show resulting calculations of seismogenic area A and segment moment rate. This example is for the northern Hayward (HN) segment and the results are from 10,000 realizations of the calculation sequence.

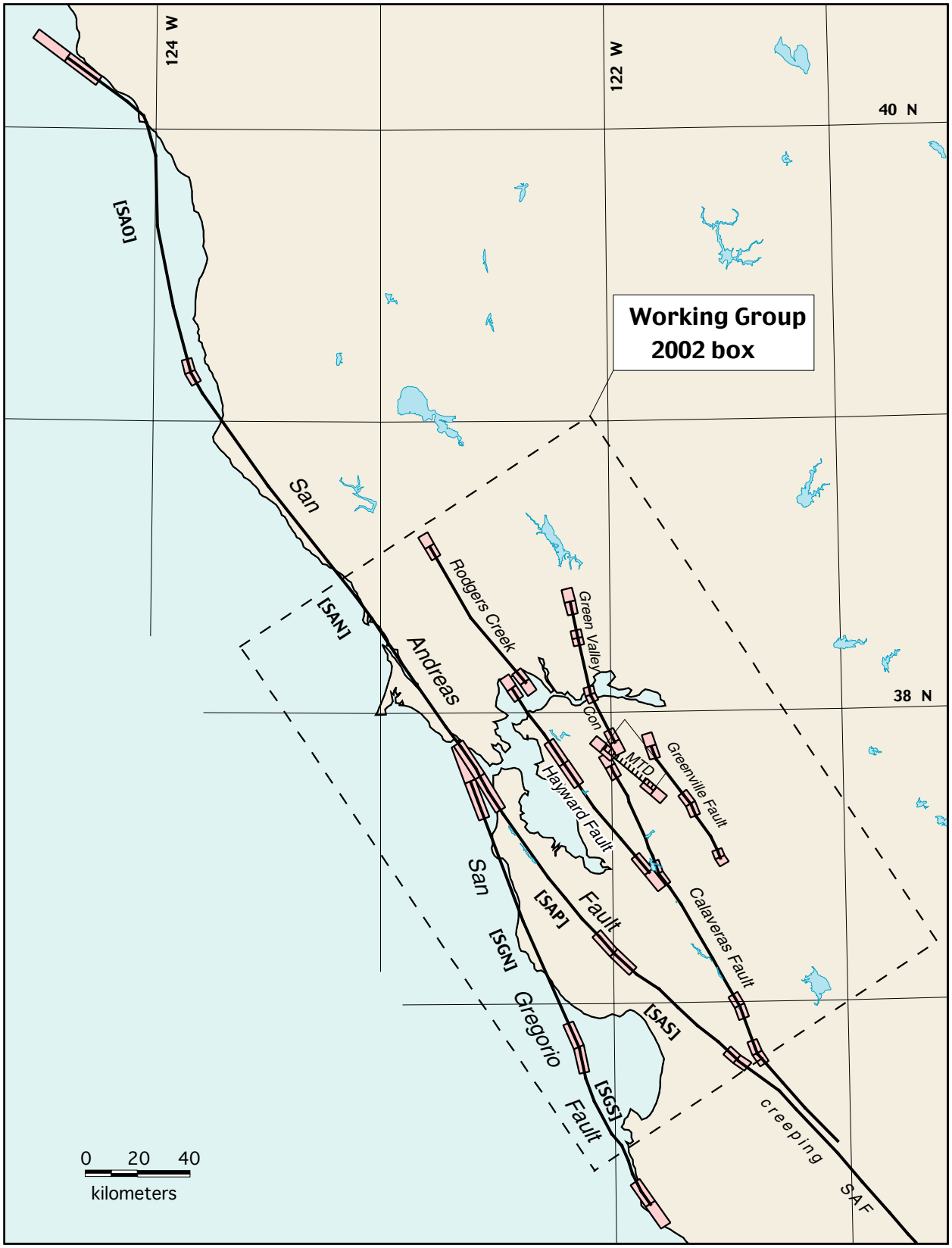

Figure 2.4, Dashed rectangle (Working Group 2002 box) shows the region included for calculation of earthquake probability and seismic moment. Bold solid lines indicate major faults for which probabilities were calculated. *MTD*, Mount Diablo Thrust; *Con*, Concord Fault. San Andreas Fault segments: SAN, North Coast; SAO, Offshore; SAP, Peninsula; SAS, Santa Cruz Mountains. San Gregorio Fault segments: SGN, North; SGS, South.

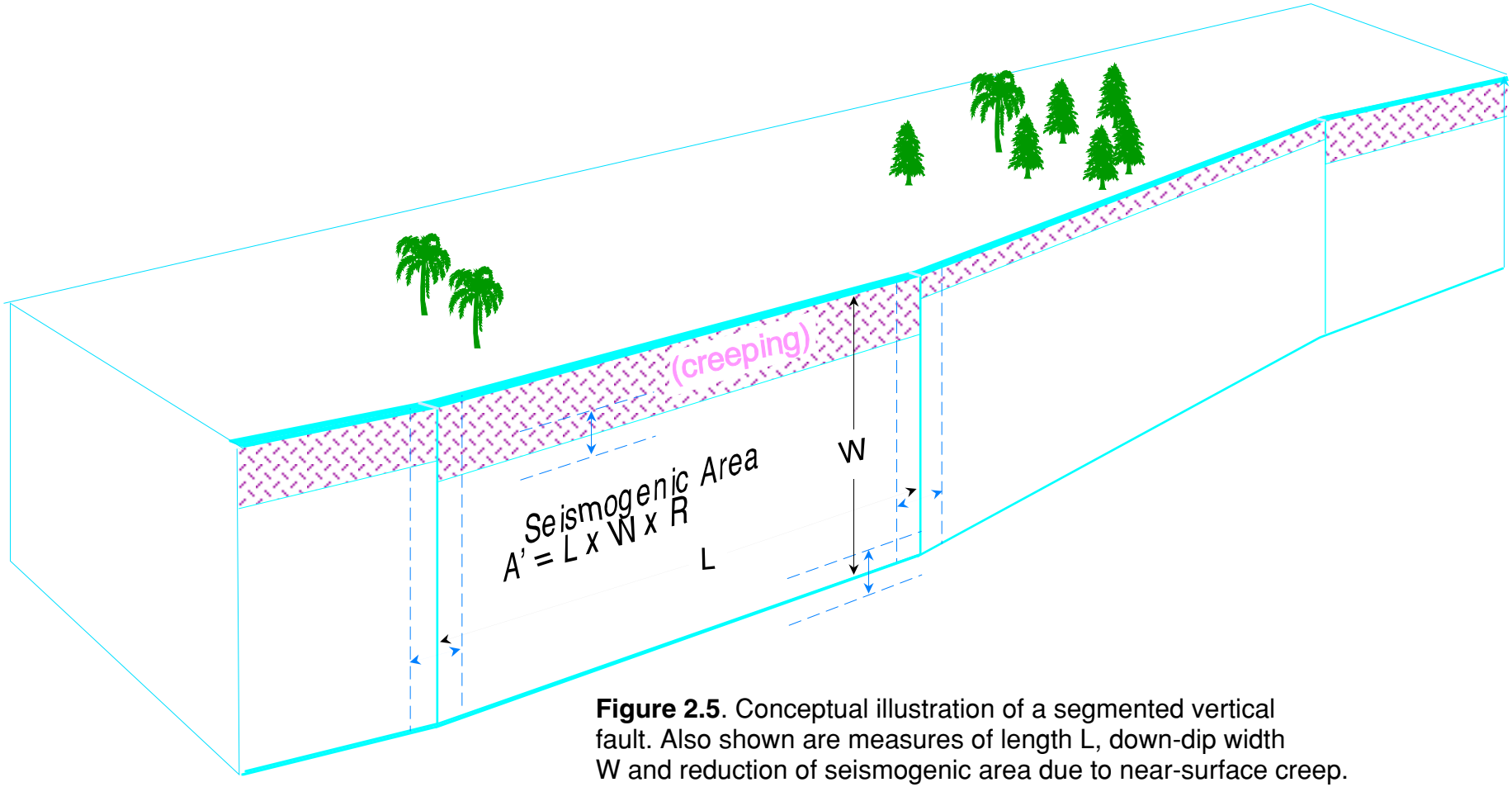

Figure 2.5. Conceptual illustration of a segmented vertical fault. Also shown are measures of length L, down-dip width W and reduction of seismogenic area due to near-surface creep. Dashed lines illustrate uncertainties in segment endpoint position and other quantities.

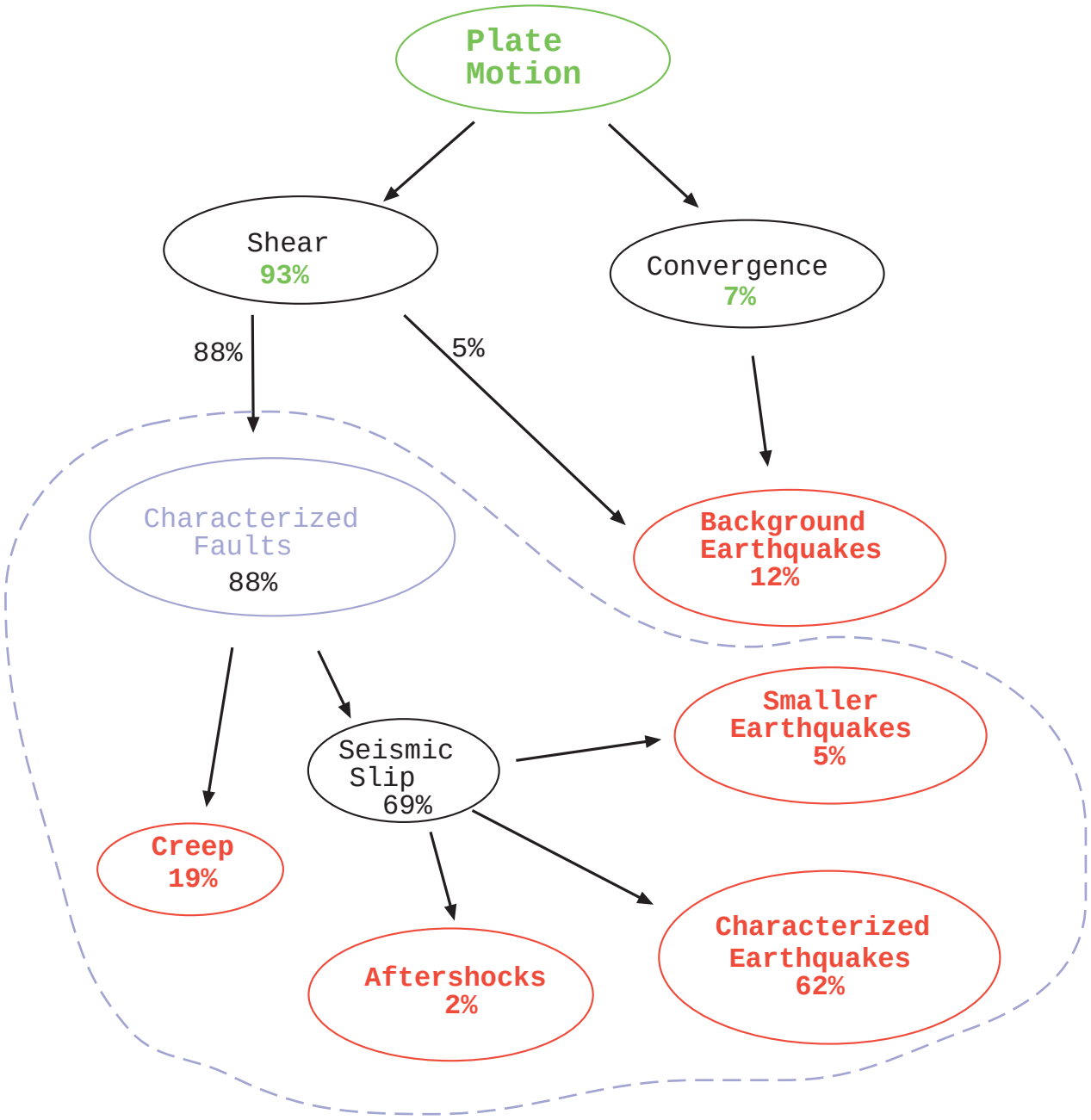

Figure 2.6. Schematic of the SFBR Earthquake Machine. The input (green) plate rate is ouput (red) as characteristic earthquakes, aftershocks, smaller earthquakes in the exponential tail, background earthquakes, and as creep. The approximate part of the total relative plate motion across the SFBR (about 2x10^18 N.m/yr of potential seismic moment) are expressed as percents. For example, the earthquake sources characterized in this report account for about 62% of the total plate motion across the SFBR.

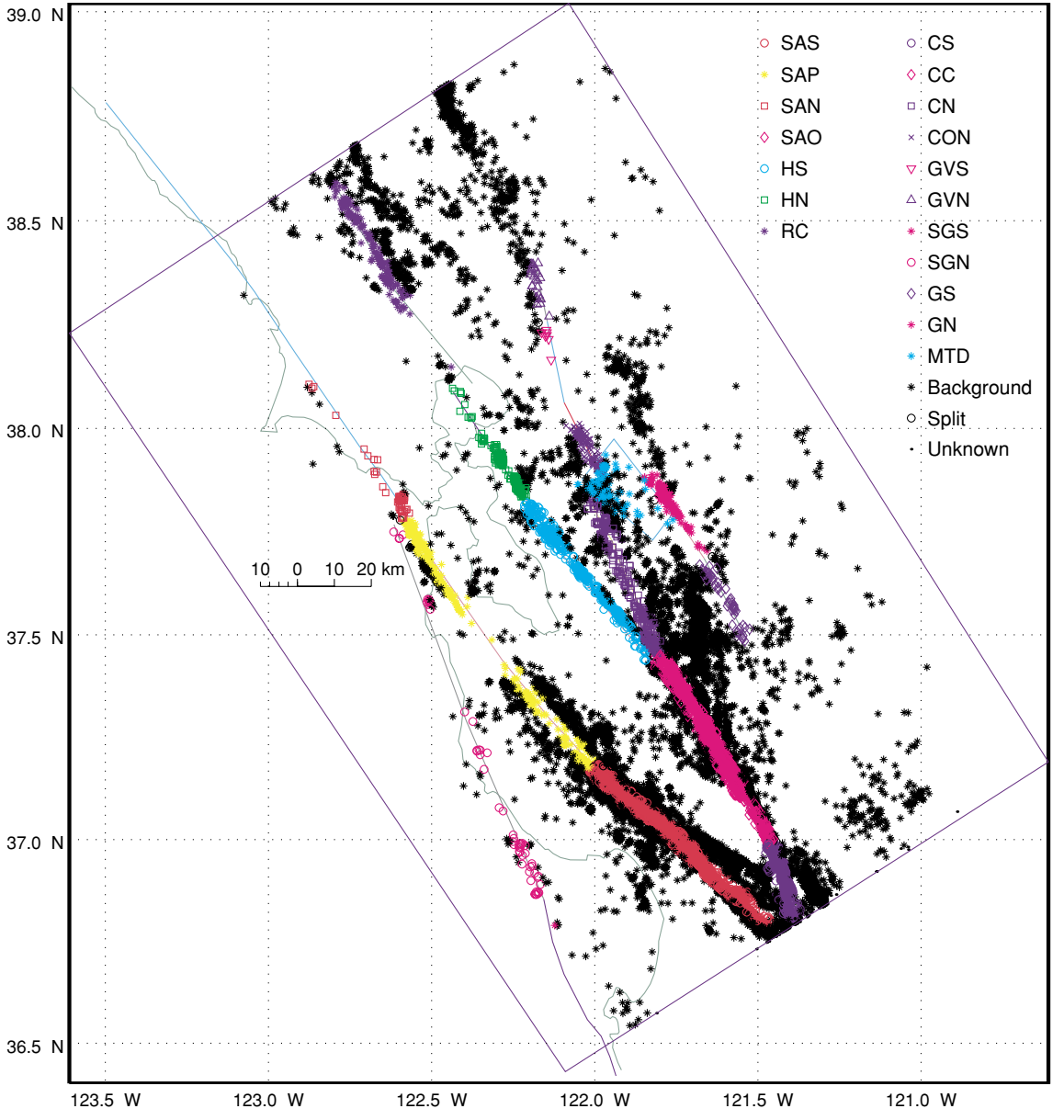

Figure 2.7. Earthquakes from the Northern California Seismic Network catalog in the SFBR. Color and symbol show the dominant probability of association with the WG02 fault segments. (Figure 9 of Wesson, et al., 2003.)

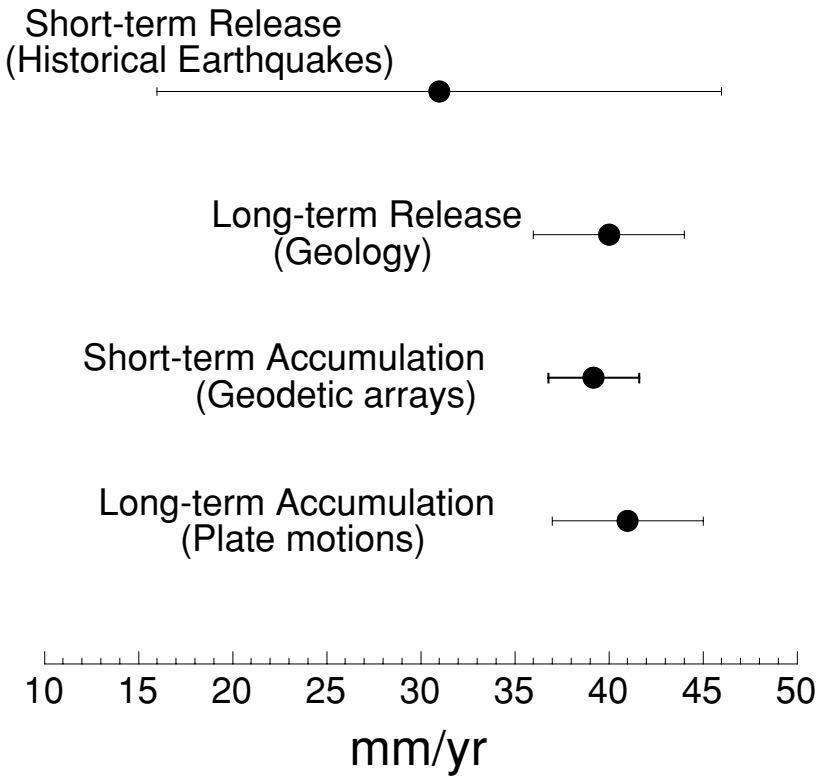

Figure 2.8. Input and output rates of slip for the SFBR earthquake machine. Error bars represent ± 2σ. The long-term and short-term accumulation rates (input to the machine) are obtained from plate-motion rates and geodetic measurements over the past few years respectively. The long-term and short-term release rates (output to the machine) are obtained from geologic slip rates and historical seismicity respectively.

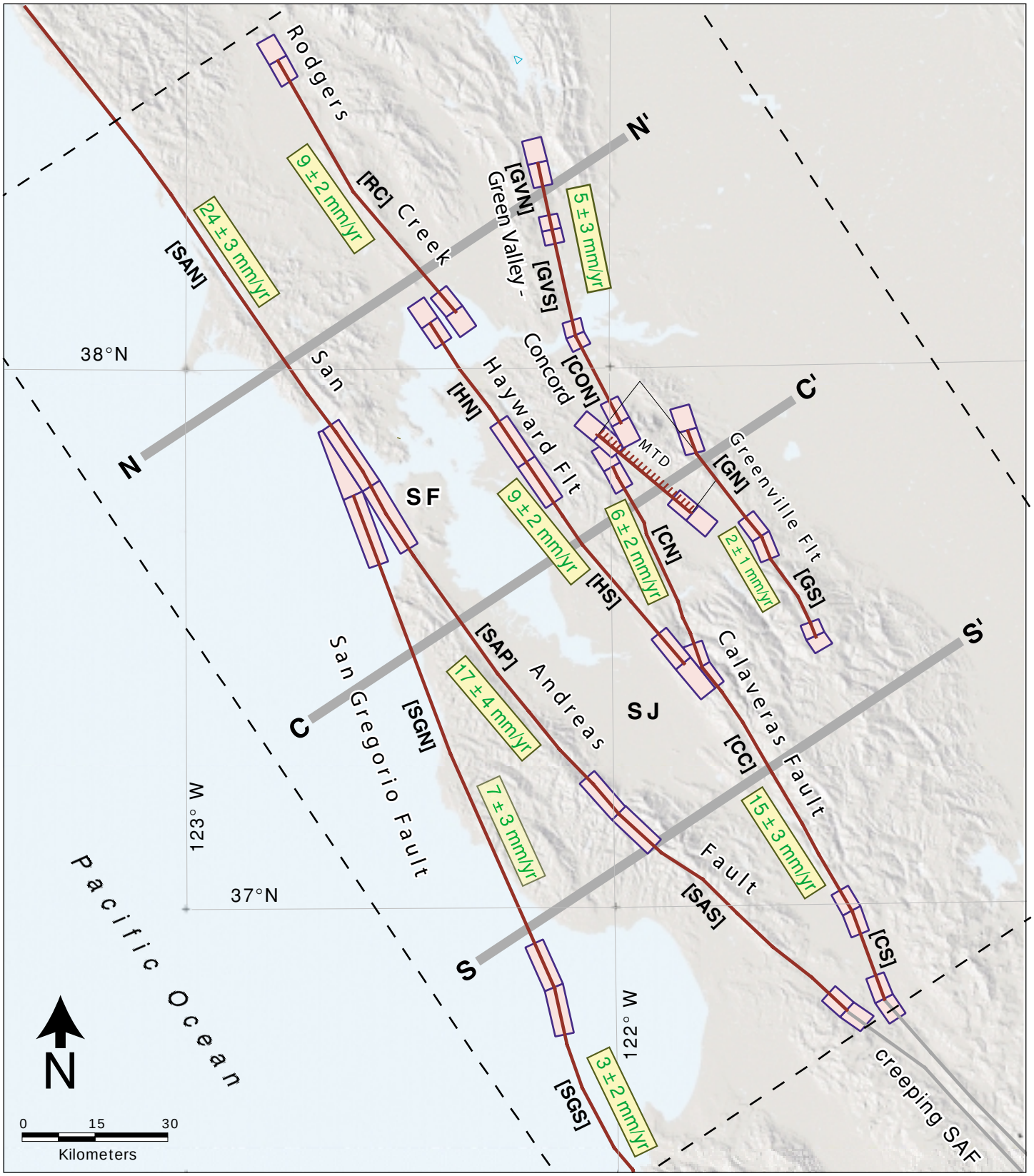

Figure 2.9, WG02 segments and slip rate. Solid gray lines tranverse to the major faults are the three transects used to sum slip rates across the region.

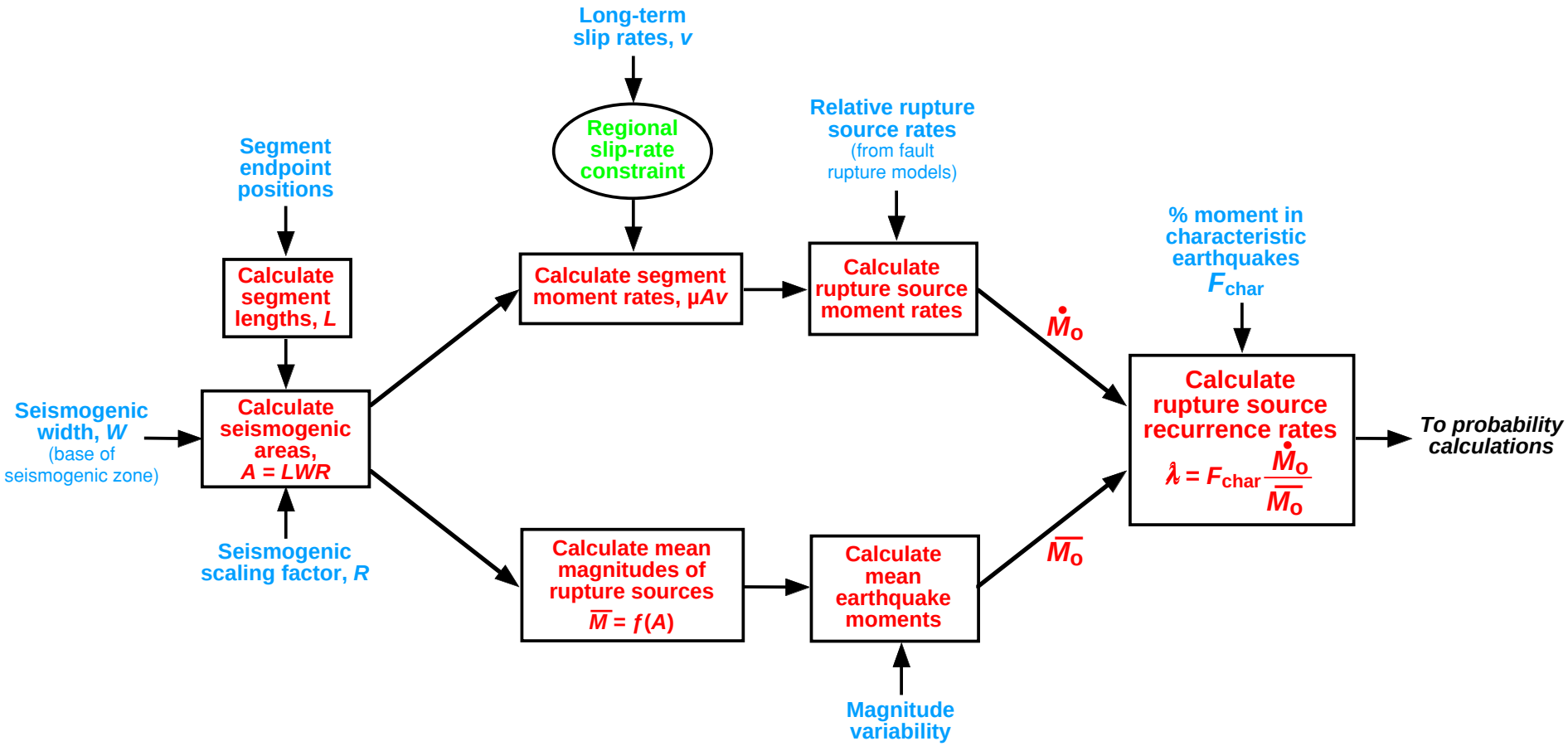

Figure 2.10. Schematic flow-chart illustrating the steps taken to calculate long-term average rupture source rates in the SFBR earthquake model. Blue text shows inputs. Boxes indicate calculation steps. The top path shows steps taken to calculate the moment rate of each rupture source. The bottom path shows the calculation of mean moment per event for those sources. The calculation in the right-most box yields the rupture source rates, which are the primary inputs to the calculation of 30-year probabilities. Not shown are the steps taken to calculate the rate of smaller earthquakes in the exponential tail, and those taken to calculate the rate of background earthquakes.

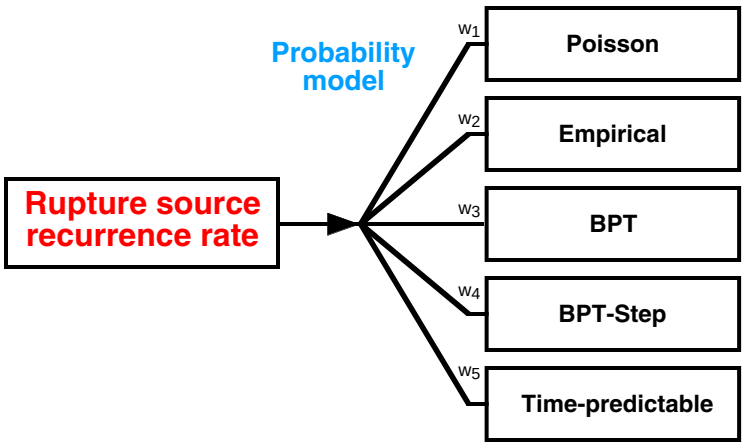

Figure 2.11. WG02 uses five alternative models for calculating probability of earthquakes in a given time interval (e.g., 2002-2031), given the long-term rate of occurrence of rupture sources. Each model requires a different set of additional information, as described in the text. Branch weights w_1–w_5 were determined by expert opinion.